

Accepted for publication in the Astronomical Journal, 06/25/02

## Observations of the Magnetic Cataclysmic Variable VV Puppis with the *Far Ultraviolet Spectroscopic Explorer*<sup>1</sup>

D. W. Hoard and Paula Szkody

*Department of Astronomy, University of Washington, Box 351580, Seattle WA 98195-1580*  
hoard, szkody@astro.washington.edu

Ryoko Ishioka

*Department of Astronomy, Faculty of Science, Kyoto University, Sakyou-ku, Kyoto, 606-8502,*  
Japan  
ishioka@kusastro.kyoto-u.ac.jp

L. Ferrario

*Department of Mathematics, Australian National University, Canberra, ACT0200, Australia*  
Lilia.Ferrario@maths.anu.edu.au

B. T. Gänsicke

*Department of Physics and Astronomy, University of Southampton, Highfield, Southampton  
SO17 1BJ, UK*  
btg@astro.soton.ac.uk

Gary D. Schmidt

*Steward Observatory, University of Arizona, 933 North Cherry Avenue, Tucson, AZ 85721-0065*  
gschmidt@as.arizona.edu

Taichi Kato and Makoto Uemura

*Department of Astronomy, Faculty of Science, Kyoto University, Sakyou-ku, Kyoto, 606-8502,*  
Japan  
tkato, uemura@kusastro.kyoto-u.ac.jp

## ABSTRACT

We present the first far-ultraviolet (FUV) observations of the magnetic cataclysmic variable VV Puppis, obtained with the *Far Ultraviolet Spectroscopic Explorer* satellite. In addition, we have obtained simultaneous ground-based optical photometric observations of VV Pup during part of the FUV observation. The shapes of the FUV and optical light curves are consistent with each other and with those of past observations at optical, extreme-ultraviolet, and X-ray wavelengths. Time-resolved FUV spectra during the portion of VV Pup's orbit when the accreting magnetic pole of the white dwarf can be seen show an increasing continuum level as the accretion spot becomes more directly visible. The most prominent features in the spectrum are the O VI  $\lambda\lambda$ 1031.9, 1037.6

emission lines. We interpret the shape and velocity shift of these lines in the context of an origin in the accretion funnel near the white dwarf surface. A blackbody function with  $T_{\text{bb}} \gtrsim 90,000$  K provides an adequate fit to the FUV spectral energy distribution of VV Pup.

*Subject headings:* accretion, accretion disks — novae, cataclysmic variables — stars: individual (VV Puppis) — stars: magnetic fields — ultraviolet: stars

## 1. Introduction

VV Puppis was noticed early in the 20th century (van Gent 1931) as a faint ( $V = 14.5$ –18; Downes et al. 2001), rapidly periodic ( $P \approx 100$  min) variable. Based on photometric and spectroscopic observations, Herbig (1960) suggested it was a binary whose emission lines originate on the brighter component. Later, VV Pup was identified as the third member of the AM Herculis class of magnetic cataclysmic variable (CV; Tapia 1977). The white dwarf (WD) primary star in an AM Her system has a magnetic field strength of  $B \gtrsim 10$  MG (currently known to reach up to several hundred MG; e.g.,  $B = 230$  MG in AR Ursae Majoris, Schmidt et al. 1999). The magnetic field prevents the formation of the accretion disk that dominates the luminosity of non-magnetic CVs. Instead, the accretion stream emerging from the low mass, main sequence secondary star’s Roche lobe is entrained onto the WD’s magnetic field lines and funneled directly onto its magnetic pole(s) (see review in Warner 1995, ch. 6). Other distinguishing characteristics of the AM Her stars include WD spin periods synchronized with their orbital periods and a high degree of linear and circular polarization (leading to the alternate name “polars” for this class of CV). Occasional reductions or interruptions to the accretion flow cause AM Her systems to drop to “low states” of reduced brightness. The origin of this accretion modulation is not fully known but may be related to, for example, solar-type magnetic activity (starspots) on the secondary star (Hessman, Gänsicke, & Mattei 2000).

Modeling of the cyclotron lines in the optical spectrum of VV Pup (which were first noted by Visvanathan & Wickramasinghe 1979 and Wickramasinghe & Visvanathan 1979) allowed Barrett & Chanmugam (1985) to estimate a magnetic field strength of  $B = 31.5$  MG at the accreting pole. The pole is located at an azimuth (i.e., the angle between the line of centers of the component stars and the projection of the magnetic axis onto the orbital plane of the CV) of  $\psi \approx 50^\circ$  and a colatitude (i.e., the angle between the rotation and magnetic axes of the WD; see Warner 1995, his Figure 6.3, for definitions of angles in polar geometry) of  $\delta \approx 150^\circ$ . Combined with a system inclination of  $i \approx 75^\circ$  for VV Pup, this pole is visible for  $\approx 45\%$  of the CV’s orbit (Cropper 1988 and

---

<sup>1</sup>Based on observations with the NASA-CNES-CSA *Far Ultraviolet Spectroscopic Explorer*. *FUSE* is operated for NASA by the Johns Hopkins University under NASA contract NAS 5-32985.

references therein). Wickramasinghe, Ferrario, & Bailey (1989) later used observations obtained during a very high accretion state to detect a  $B = 56$  MG field at the second magnetic pole, which forms an off-center dipole with the weaker first pole. Despite being weaker, the location of the first pole on the synchronously rotating WD – on the side facing the secondary star – makes it the preferred site for the accretion flow. However, accretion onto the second pole (which is located within  $\approx 10^\circ$  of the WD rotation axis, so is always visible; Wickramasinghe, Ferrario, & Bailey 1989) sometimes also occurs, as evidenced by polarimetric observations made when the first pole is not visible (due to orbital motion) and differences in the total system brightness when the first pole is inactive ( $V \approx 16$  when the second pole is active vs.  $V \approx 18$  when both poles are inactive; e.g., Liebert & Stockman 1979). A blackbody fit to the optical spectrum of VV Pup during an extended, steady low state (both poles inactive) in 1977 suggested a temperature of  $\approx 9000$  K for the WD (Liebert et al. 1978).

VV Pup has been extensively observed at infrared (Szkody, Bailey, & Hough 1983), optical (Warner & Nather 1972; Imamura, Steiman-Cameron, & Wolff 2000), ultraviolet (Patterson et al. 1984), extreme-ultraviolet (EUV; Vennes et al. 1995), and X-ray (Patterson et al. 1984; Imamura, Steiman-Cameron, & Wolff 2000) wavelengths. The EUV data indicated a possible oxygen over-abundance and the presence of a hot accretion region. To further study these properties of VV Pup, we obtained the first far-ultraviolet (FUV) observation of this magnetic CV, with the *Far Ultraviolet Spectroscopic Explorer (FUSE)* satellite.

## 2. Observations

We observed VV Pup with *FUSE* during 11 visits between HJD 2452004.5–2452005.3 (2001 April 05, 00:28–17:08 UT; see Table 1). The start time of each visit was selected to correspond to approximately the same orbital phase of the CV in successive cycles, in order to facilitate co-adding data spanning  $\approx 40\%$  of the CV’s orbit. All visits utilized the LWRS aperture and TTAG accumulation mode (for *FUSE* spacecraft and instrument details see, e.g., Sahnow et al. 2000)<sup>2</sup>. Details of the FUV data processing are given in Sections 2.1 and 2.3.

### 2.1. Far-ultraviolet Light Curves

We used the CalFuse v2.0.5 software to extract time-resolved spectra from the raw data files obtained during each *FUSE* visit, in successive 200-s intervals starting at the beginning of each visit. Remaining exposure intervals of less than 200 s at the end of any visit were not used. We then used a custom-built IDL routine (following the recipes in the *FUSE* Data Analysis Cookbook<sup>3</sup>)

---

<sup>2</sup>Also see the *FUSE* Science Center web page at <http://fuse.pha.jhu.edu/>.

<sup>3</sup>See <http://fuse.pha.jhu.edu/analysis/cookbook.html>.

to combine the various mirror and detector segments of the spectra. Because the spectra were very weak, exceptions to the standard Cookbook procedures were made as follows: (1) only the LiF data ( $\lambda \gtrsim 980$  Å) were used (the SiC data are very noisy, with little apparent signal) and (2) no wavelength cross-correlation or shifts between different exposures were applied. There is a small gap in the wavelength coverage between 1082–1087 Å where only SiC data are available. In addition, the LiF1 data for  $\lambda > 1133$  Å were not used in order to avoid the artifact known as “The Worm” (only the LiF2 data in this region are used). The final combined spectra were rebinned onto a uniform wavelength scale with dispersion  $0.05$  Å pixel $^{-1}$  by averaging flux points at the original dispersion into wavelength bins of width  $0.05$  Å.

In this manner, a total of 87 time-resolved spectra were extracted from the 11 *FUSE* visits. These spectra are too weak and noisy to be useful in their dispersed form; instead, we summed the flux values in the wavelength ranges (A) 1000.0–1024.5 Å + 1045.0–1080.0 Å + 1088.0–1160.0 Å, and (B) 1028.5–1045.0 Å. Both of these ranges were chosen to avoid the extremely noisy short wavelength ( $\lambda < 1000$  Å) data, a strong airglow feature at the location of Ly- $\beta$ , and the detector gap mentioned above. Wavelength region A includes primarily continuum with only a few weak line features (and excludes region B), while region B includes only the O VI  $\lambda\lambda 1031.9, 1037.6$  lines (the O I  $\lambda\lambda 1039.2, 1040.9$  lines are also included – these are probably airglow features, but they are relatively weak compared to the O VI lines, so should contribute little to the total flux in this wavelength region). We henceforth refer to these data as (A) continuum and (B) emission.

Figure 1 shows the FUV light curves constructed from the summed spectra. Orbital phases were calculated using the ephemeris of Walker (1965); we note that this ephemeris defines the phase of maximum (optical) light as its zero point. Infrared observations (Szkody & Capps 1980; Szkody, Bailey, & Hough 1983; also see the geometric model in Patterson et al. 1984, their Figure 8) show that the inferior conjunction of the secondary star (normally used as the orbital phase zero point) occurs at  $\phi \approx 0.1$  according to the Walker (1965) ephemeris. This amount may be subtracted from the phases quoted in this paper to approximate the “standard” relationship between orbital phase and system geometry for CVs. The continuum flux in our *FUSE* light curve starts at zero at phase  $\phi \approx 0.7$ , increases substantially to a maximum at  $\phi \approx 0.98$ , then appears to begin declining at later phases. The emission flux approximately follows the continuum pattern, almost doubling its mean amplitude at the start of the light curve by the time it reaches  $\phi \approx 0.98$ . However, the rate of increase and subsequent leveling off is more gradual than displayed by the continuum data. The continuum fluxes were summed over a wavelength region  $\approx 6$  times larger than the emission fluxes, so their absolute flux levels as shown in Figure 1 cannot be directly compared to each other. However, even after accounting for this difference, the slope of the continuum light curve (obtained by approximating the curve as a linear function) over the phase range  $\phi = 0.70$ – $0.98$  is more than twice that of the same section of the emission light curve.

## 2.2. Optical Light Curve

We also obtained ground-based optical observations of VV Pup on 2001 April 05, overlapping with *FUSE* visit 7 (ending just prior to the start of *FUSE* visit 8). These data were acquired using an unfiltered ST-7 CCD on a 25-cm telescope. Each measurement had an exposure time of 30 s, and the entire time series spanned 0.0775 d (1.86 hr). We calculated instrumental magnitudes and statistical uncertainties from the net background-subtracted count rates in each exposure for VV Pup and several nearby field stars. Figure 2 shows the differential light curve of VV Pup with respect to a comparison star. The differential light curve of another field star and the same comparison star is also shown to illustrate the intrinsic noise level of the measurements ( $\sigma_{\text{diff}} = 0.046$  mag). According to the USNO A1.0 catalog, our comparison star (USNO 0675-06141640) has blue and red magnitudes of 13.8 and 12.6, respectively. Thus, VV Pup was fainter than  $\approx 16.5$  mag at orbital phases away from the hump in the light curve, indicating that the second magnetic pole was not accreting during our *FUSE* observation. The larger scatter at each end of the VV Pup light curve is caused by poor- or non-detection of the CV during orbital phases when it is not bright (i.e., when the accreting magnetic pole has rotated out of view).

The overall shape of our optical light curve is very similar to that of the optical light curve of VV Pup in Patterson et al. (1984) and the EUV light curve in Vennes et al. (1995). The latter authors note that the ephemeris of Walker (1965) is good to within  $\pm 0.05$  orbital cycles at the epoch of their data (1993). Following this reasoning, we would expect that the phasing of our 2001 epoch data is good to better than  $\approx \pm 0.07$  cycles. However, comparison of the phasing of the bright hump in our optical light curve with the published light curves listed above (especially in Patterson et al. 1984, their Figure 3) suggests that the accumulated offset in the phasing of the Walker (1965) ephemeris is less than  $\pm 0.07$ , and likely still as small as  $\approx \pm 0.05$ .

Figure 3 shows a comparison of the FUV and optical light curves of VV Pup. The top panel shows our optical data as a function of HJD; we have overplotted the *FUSE* data that exactly match the time of the optical observations. It is already clear that the optical and FUV continuum data behave similarly, while the FUV emission data display substantially different behavior from the optical data. The bottom panel in the figure shows the optical and FUV continuum data folded on the ephemeris of Walker (1965). There is good agreement between the light curve shapes of the folded optical and FUV continuum data.

As mentioned above, our optical light curve is very similar in phasing and overall appearance to the optical light curve of VV Pup in Patterson et al. (1984): it begins to rise from the “zero” level at an approximately constant rate at  $\phi \approx 0.70$ , reaches maximum at  $\phi \approx 0.05$ , levels off until  $\phi \approx 0.15$ , and then drops steeply back to the zero level in only a few hundredths of an orbital cycle. The FUV continuum light curve, however, appears to peak and already begin declining well before the optical peak, and also well before the peak found in a light curve obtained from the *Extreme Ultraviolet Explorer (EUVE)* satellite (Vennes et al. 1995, their Figure 2). It is possible that this is caused by the accretion stream occultation feature suggested by Vennes et al. (1995), but we

cannot make a firm conclusion without having *FUSE* data from later orbital phases.

### 2.3. Far-ultraviolet Spectrum

We used the procedure described in Section 2.1 and the ephemeris of Walker (1965) to extract three additional time-resolved spectra from the raw *FUSE* data. Data from each of the 11 *FUSE* visits corresponding to orbital phase ranges of  $\Delta\phi_1 = 0.67\text{--}0.79$  (total exposure time of 7069 s),  $\Delta\phi_2 = 0.80\text{--}0.89$  (5442 s), and  $\Delta\phi_3 = 0.90\text{--}0.06$  (5929 s) were combined to produce these spectra (see Figure 4). They have weak, mostly flat continua with a “hump” between  $\approx 1010\text{--}1050$  Å. The spectra lack prominent emission or absorption features with the exception of several O I and O VI emission lines around 1030 Å (identified in Section 2.1) and a C III emission feature at 1175 Å. The wavelengths of a few lines of other ions are identified in Figure 4, but they are not entirely convincing as real features.

As is reflected in the FUV light curve of VV Pup (see Section 2.1), the continuum flux level in the spectra increases at larger orbital phases. Despite significant changes in the shapes of the O VI emission line profiles (it is arguable whether these lines are even still present in the  $\Delta\phi_3$  spectrum), the total flux in this wavelength region remains relatively constant (compared to the continuum flux change – see Figure 1). The narrow O I lines seen in the  $\Delta\phi_1$  spectrum are probably airglow features, since approximately 65% of the combined data for this spectrum were obtained during spacecraft day (all of the  $\Delta\phi_2$  and  $\Delta\phi_3$  data, which do not show the O I emission, were obtained during spacecraft night). The prominence of the O VI features in the spectrum of VV Pup may be related to the possible oxygen overabundance suggested by Vennes et al. (1995) from their EUV data. On the other hand, a recent *FUSE* spectrum of the prototype magnetic CV, AM Her, also shows strong O VI emission (Hutchings et al. 2002), so this may be a common FUV feature of magnetic CVs (or CVs in general). We do not observe narrow emission components in the O VI profiles of VV Pup, as seen by Mauche (1999) in *ORFEUS II* FUV spectra of the polar EX Hydrael, and by Mauche & Raymond (1998) and Hutchings et al. (2002) in *ORFEUS II* and *FUSE* spectra, respectively, of AM Her. In the case of EX Hya, the narrow component velocities suggest an origin on the WD, whereas in AM Her, the velocities suggest an origin on the irradiated inner face of the secondary star. Given that these narrow emission components can originate from very different regions in these two polars, it is not so surprising that they might be absent altogether in a third polar.

### 3. Discussion

#### 3.1. System Geometry

We can use the geometric model for VV Pup presented by Patterson et al. (1984) to estimate which system components are visible along the lines-of-sight represented by each of our phase-resolved *FUSE* spectra. The phase interval  $\Delta\phi_1$  starts shortly after the superior conjunction of the secondary star (signaled by a photometric infrared minimum) at  $\phi \approx 0.6$ . Optical circular polarization appears at  $\phi \approx 0.75$  as the accretion spot on the WD first becomes visible. The accretion funnel is visible earlier, possibly for the entire  $\Delta\phi_1$  interval. The broad O VI emission lines present in the  $\Delta\phi_1$  spectrum display little or no Doppler shift, and likely originate in the accretion funnel, which is directed approximately perpendicular to the observer’s line-of-sight during most of this phase interval. These are high excitation lines and, hence, most likely are formed in the hot portion of the funnel, close to the WD surface (henceforth, we refer to this as the “inner funnel” to signify its proximity to the WD in the CV system).

The phase interval  $\Delta\phi_2$  brackets the phase of maximum elongation, when the WD (secondary star) is maximally receding from (approaching) the observer. The accretion funnel is now viewed in recession from the observer, due to both the binary motion of the WD and the matter flow motion within the funnel. This motion is reflected in the redward shift of the O VI line peaks compared to the previous spectrum. In addition, the oxygen lines are weaker than in the  $\Delta\phi_1$  spectrum, possibly because the cooler outer part of the accretion funnel is partially obscuring the hotter part closer to the WD where the O VI lines presumably originate (however, see the discussion below).

The phase of maximum optical/UV light occurs in  $\Delta\phi_3$  at  $\phi \approx 0.98$ , when the magnetic pole of the WD and associated accretion spot (located at an azimuth of  $\psi \approx 50^\circ$ ; Cropper 1988) rotates fully and directly into view. We would, thus, expect emission from the high velocity inner end of the accretion funnel to have maximum redshift in this phase interval. Unfortunately, the O VI emission lines appear to have essentially disappeared in the phase-resolved spectrum. The inclination ( $i \approx 75^\circ$ ) and magnetic pole colatitude ( $\delta \approx 150^\circ$ ) in VV Pup (Cropper 1988) make it unlikely that this is the result of complete obscuration of the emission region in the hot inner funnel by another part of the funnel, unless the obscuring funnel material is located far from the WD surface (see discussion in Patterson et al. 1984, their Section IIIb). Additionally, this would only be expected to affect the system for a short time (e.g., to produce the narrow dip seen by Vennes et al. 1995 in the EUV light curve of VV Pup). The FUV emission light curve (see Figure 1) shows that the flux in the wavelength region around the oxygen lines increases during  $\Delta\phi_3$ , contrary to our expectation if the emission lines were suddenly blocked from view during this orbital phase interval. In addition, the  $\Delta\phi_3$  spectrum displays a broad hump where the O VI line peaks were located in the  $\Delta\phi_2$  spectrum. The red edge of this hump is located considerably redward (at  $\approx 1043$  Å) of the red edge of the O VI  $\lambda 1037.6$  line in the  $\Delta\phi_2$  spectrum (at  $\approx 1039$  Å). A similar effect was seen by Ferrario & Wehrse (1999) in the emission lines of model optical spectra for a high inclination polar near the phase of maximum redshift (e.g., their Figure 10). They attributed it to

a combination of velocity smearing and self-obscurcation in the funnel. Thus, we suggest that the O VI emission lines are still present and visible in the  $\Delta\phi_3$  spectrum of VV Pup, but they have been both substantially redshifted and severely broadened, to the point of being unrecognizable as peaked emission line profiles, by our “deepest” view down the accretion funnel to its inner, high velocity end.

### 3.2. Accretion Region Characteristics

VV Pup was observed several times with the *International Ultraviolet Explorer (IUE)* satellite (e.g., Patterson et al. 1984). We extracted the available data from the *IUE* archive, and have plotted a representative short wavelength spectrum (SWP07868, 14,400 s obtained on 1980 February 04) and the only long wavelength spectrum (LWR07309, 7200 s obtained on 1980 March 26) in Figure 5. A mean FUV spectrum constructed by combining our three phase-resolved spectra of VV Pup is also shown in the figure. The flux levels of all three satellite spectrum segments agree well at their boundaries (despite the fact that the *IUE* spectra are each averaged over several orbital cycles of the CV, whereas the combined *FUSE* spectrum covers only  $\Delta\phi \approx 0.40$  during the brightest portion of the orbit).

In Figure 6, we have overplotted three simple models onto a *FUSE*+*IUE* spectrum of VV Pup. The same *IUE* data from Figure 5 are used, but the  $\Delta\phi_3$  (i.e., strongest continuum) *FUSE* spectrum is used instead of the mean spectrum. The models are: a power law of the form  $F_\lambda \propto \lambda^\alpha$  where  $\alpha = -2$  or  $-4$ , and a blackbody function with  $T_{\text{bb}} = 90,000$  K. The inset panel of the figure shows the models with only the *FUSE* data; the horizontal bars mark the wavelength regions used to normalize the three models. In the case of the power law, the exponent was kept fixed and the multiplicative scaling factor that minimized the r.m.s. deviation between the data and the fit was determined. A similar process was followed for the blackbody fit: the normalization with minimum r.m.s. was determined for fixed temperatures in 5000 K steps in the range 50,000–500,000 K, and we kept the model with the overall smallest r.m.s. deviation. (The r.m.s. values increase smoothly on either side of the model with  $T_{\text{bb}} = 90,000$  K.) All three of these models provide adequate fits to the continuum shape of the phase-resolved *FUSE* spectrum within the relatively loose limits allowed by its low S/N. By comparison, a 9000 K WD (Liebert et al. 1978) would contribute very little flux in the FUV (a factor of  $\approx 6 \times 10^{-5}$  smaller than the 90,000 K blackbody at 1100 Å). The *IUE* data were not used when we determined the model normalizations. Yet, the  $\alpha = -4$  power law and hot blackbody both still provide good fits to the data when extended into the *IUE* spectra. Assuming that the normalization to the *FUSE* data is correct, then the *IUE* data effectively rule out the  $\alpha = -2$  power law (equivalent to cooler temperatures) as a good fit to the UV spectral energy distribution of VV Pup.

Vennes et al. (1995) estimated an accretion region temperature of 300,000 K from WD synthetic spectrum fits to their *EUVE* spectrum of VV Pup. Although hotter than the nominal temperature found from a blackbody fit to our *FUSE* data, the *EUVE* result is not inconsistent with the *FUSE*

data – a 300,000 K blackbody would produce a curve almost indistinguishable from the  $\alpha = -4$  power law. We expect to find a lower temperature in our data since we have moved to longer wavelengths, and are presumably observing cooler zones of a more extended accretion region than is detectable in the EUV (the *EUVE* spectrum covers  $\approx 80$ –140 Å compared to  $\approx 1000$ –1180 Å for *FUSE*). Gänsicke (1997) found a range of accretion spot temperatures of  $\approx 25,000$ –40,000 K in a sample of seven AM Her systems using ultraviolet (1200–3000 Å) data from *IUE*. Thus, our best model temperature of 90,000 K lies between the temperatures derived from longer wavelength *IUE* data and shorter wavelength *EUVE* data, as expected.

The flux of our 90,000 K blackbody model at  $\lambda = 5500$  Å is  $F_{5500} \approx 1.7 \times 10^{-17}$  erg s $^{-1}$  cm $^{-2}$  Å $^{-1}$ . Using  $F_{5500} \approx 3.7 \times 10^{-9}$  erg s $^{-1}$  cm $^{-2}$  Å $^{-1}$  for a 0th magnitude AOV star (Colina, Bohlin, & Castelli 1996), then the magnitude of our 90,000 K blackbody model at  $\lambda = 5500$  Å would be  $\approx 20.8$ , much fainter than the optical magnitude of  $\approx 16.5$  determined for VV Pup from our ground-based data (see Section 2.2). In this regard, it is unclear why the optical and FUV–EUV light curves of VV Pup are so similar in appearance, since the dominant source of FUV flux does not contribute significantly at optical wavelengths. Reprocessing of the FUV radiation in material around the accretion region may play a role in this.

The normalization factor ( $N = 4\pi r^2/d^2 = 1.13 \times 10^{-25}$ ) determined for the 90,000 K blackbody model corresponds to a circular emitting region with radius given by

$$r_{\text{acc}} \approx (293 \text{ km})(d/100 \text{ pc}), \quad (1)$$

where  $d$  is the distance to VV Pup in pc. This gives  $r_{\text{acc}} \approx 425$  km for  $d = 145$  pc (Bailey 1981; Vennes et al. 1995). We would expect that the detectable accretion region should be somewhat larger in the FUV than in the EUV (because we are able to detect radiation from cooler regions), and this estimate is  $\approx 4$  times the  $r_{\text{acc,EUV}} = 110$  km obtained by Vennes et al. (1995) from timing and geometric considerations using a 3-d hemispherical spot model (unfortunately, we lack the necessary timing information to repeat their 3-d calculation because of the incomplete coverage of the bright hump in our FUV light curve). A hotter blackbody model would require a larger normalization factor (thus yielding a smaller  $r_{\text{acc}}$  for the same distance); for example, if  $T_{\text{bb}} = 300,000$  K, then  $N = 2.7 \times 10^{-26}$  and  $r_{\text{acc}} \approx 210$  km. By comparison, the 9000 K WD found by Liebert et al. (1978) would need a radius of almost 55,000 km to account for the observed FUV flux of VV Pup at a distance of 145 pc (or be located at a distance of only  $\approx 15$  pc if the WD radius is a more reasonable 6000 km).

#### 4. Conclusions

Analysis of our *FUSE* observations of VV Pup has revealed many of the FUV characteristics of this magnetic CV. The shape of the FUV light curve is consistent with that seen at other wavelengths (optical, EUV, X-ray). Likewise, the characteristics of the phase-resolved FUV spectra during the bright portion of VV Pup’s orbit (when the accreting magnetic pole is visible) agree

with expectations from the geometric model for this system presented by Patterson et al. (1984). These include an increase in the continuum level at later orbital phases (as the magnetic pole and its associated accretion region rotate into more direct view) and changes in the shape and velocity shift of the prominent O VI emission lines that we interpret in the context of the lines originating in the high velocity, hot, inner region of the accretion funnel located close to the WD surface. A hot temperature ( $T \gtrsim 90,000$  K) is favored for a simple model of the FUV spectral energy distribution in VV Pup, in terms of both the fit to the *FUSE* and archival *IUE* continuum in the wavelength range 1000–3000 Å, and the size of the accretion region estimated from the normalization of the model. Although we expect *a priori* that observations in the FUV should detect a cooler (and more extended) accretion region than did the *EUVE* observations of Vennes et al. (1995), we cannot rule out a temperature as high as the 300,000 K determined for the EUV as an adequate fit to the *FUSE* data.

We thank Paul Barrett for his input regarding the *FUSE* spectrum of VV Pup. This work was supported by NASA *FUSE* grant NAG 5-10343. B. T. G. was supported by a PPARC Advanced Fellowship. We made use of the SIMBAD database, operated at CDS, Strasbourg, France.

## REFERENCES

Bailey, J. 1981, MNRAS, 197, 31

Barrett, P. E., Chanmugam, G. 1985, ApJ, 298, 743

Colina, L., Bohlin, R., Castelli, F. 1996, Space Telescope Science Institute Observatory Support Group Calibration Report, OSG-CAL-96-01<sup>4</sup>

Cropper, M. 1988, MNRAS, 231, 597

Downes, R. A., Webbink, R. F., Shara, M. M., Ritter, H., Kolb, U., Duerbeck, H. W. 2001, PASP, 113, 764

Feldman, P. D., Sahnow, D. J., Kruk, J. W., Murphy, E. M., Moos, H. W. 2001, J. Geophys. Res., 106, 8119

Ferrario, L., Wehrse, R. 1999, MNRAS, 310, 189

Gänsicke, B. T. 1997, PhD thesis (U. of Göttingen)

Herbig, G. H. 1960, ApJ, 132, 76

Hessman, F. V., Gänsicke, B. T., Mattei, J. A. 2000, A&A, 361, 952

---

<sup>4</sup>See <http://www.stsci.edu/instruments/observatory/reports.html>.

Hutchings, J. B., Fullerton, A. W., Cowley, A. P., Schmidtke, P. C. 2002, AJ, 123, 2841

Imamura, J. N., Steiman-Cameron, T. Y., Wolff, M. T. 2000, PASP, 112, 18

Liebert, J., Stockman, H. S. 1979, ApJ, 229, 652

Liebert, J., Stockman, H. S., Angel, J. R. P., Woolf, N. J., Hege, K., Margon, B. 1978, ApJ, 225, 201

Mauche, C. W. 1999, ApJ, 520, 822

Mauche, C. W., Raymond, J. C. 1998, ApJ, 505, 869

Patterson, J., Beuermann, K., Lamb, D. Q., Fabbiano, G., Raymond, J. C., Swank, J., White, N. E. 1984, ApJ, 279, 785

Sahnow, D. J., et al. 2000, Proc. SPIE, 4013, 334

Schmidt, G. D., Hoard, D. W., Szkody, P., Melia, F., Honeycutt, R. K., Wagner, R. M. 1999, ApJ, 525, 407

Szkody, P., Bailey, J. A., Hough, J. H. 1983, MNRAS, 203, 749

Szkody, P., Capps, R. W. 1980, AJ, 85, 882

Tapia, S. 1977, IAU Circ., 3054, 1

van Gent, H. 1931, Bull. Astron. Inst. Netherlands, 6, 93

Vennes, S., Szkody, P., Sion, E. M., Long, K. S. 1995, ApJ, 445, 921

Visvanathan, N., Wickramasinghe, D. T. 1979, Nature, 281, 47

Walker, M. F. 1965, Comm. Konkoly Obs., 57, 1

Warner, B. 1995, Cataclysmic Variable Stars (Cambridge: Cambridge University Press)

Warner, B., Nather, R. E. 1972, MNRAS, 156, 305

Wickramasinghe, D. T., Ferrario, L., Bailey, J. 1989, ApJ, 342, L35

Wickramasinghe, D. T., Visvanathan, N. 1979, Proc. Astron. Soc. Australia, 3, 311

Table 1. *FUSE* Observation Log

Visit	Start Time (HJD–2450000)	Total Exposure (s)	$\phi^a$
1	2004.52312	501	0.721
2	2004.59228	741	0.712
3	2004.66153	981	0.705
4	2004.73099	1310	0.701
5	2004.80044	1770	0.697
6	2004.86983	2180	0.692
7	2004.93937	2270	0.689
8	2005.00881	2270	0.684
9	2005.07812	2270	0.678
10	2005.14751	2271	0.673
11	2005.21740	2014	0.675

<sup>a</sup>Orbital phase at start of exposure from the ephemeris of Walker (1965).

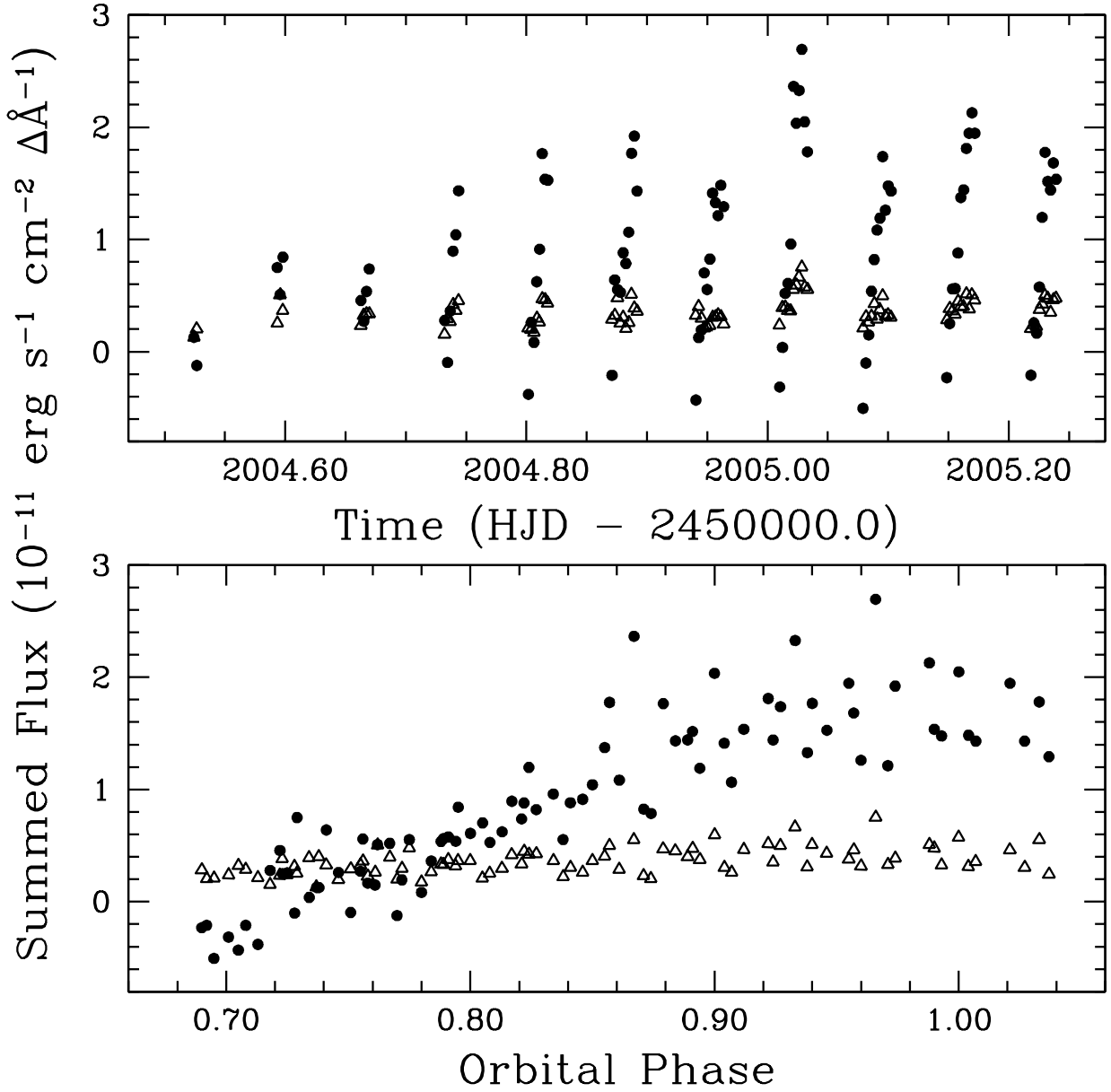


Fig. 1.— FUV light curves of VV Pup constructed by summing fluxes in 200-s time-resolved *FUSE* spectra (see text for wavelength regions summed). The continuum fluxes are plotted as filled circles; the oxygen emission line fluxes are plotted as unfilled triangles. The top panel shows the data as a function of time, while the bottom panel shows the data folded on the orbital ephemeris of Walker (1965). The 11 individual *FUSE* visits are apparent in the top panel.

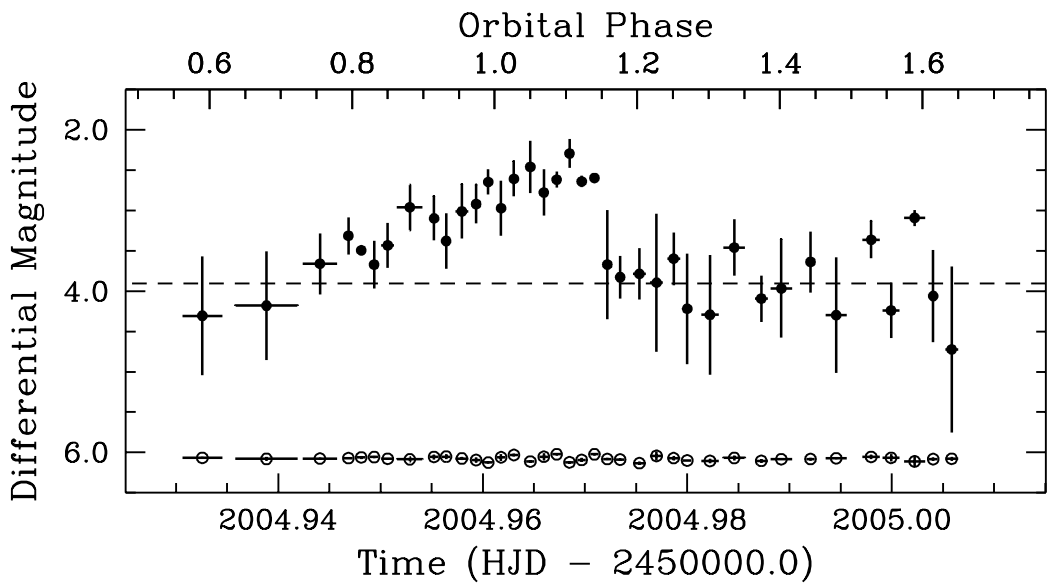


Fig. 2.— Optical differential light curve of VV Pup and a comparison star (filled circles), averaged into bins of 3 data points each. The vertical error bars are the standard deviations of the means of each 3-point bin, while the horizontal bars show the width in time and phase of each bin. The unfilled circles are the differential light curve of another field star and the same comparison star (offset by +6.0 mag for clarity and also binned by 3 points);  $1\sigma$  vertical error bars are also plotted for the comparison star light curve, but they are smaller than the data points at the scale of the plot. The lower x-axis scale gives the heliocentric Julian date, while the upper x-axis scale gives the orbital phase of VV Pup from the ephemeris of Walker (1965). The dashed line shows the effective zero level of the VV Pup light curve – it is located at  $y = 3.903$  mag, which is the mean of the VV Pup differential magnitudes for  $\text{HJD} > 2452004.9725$ .

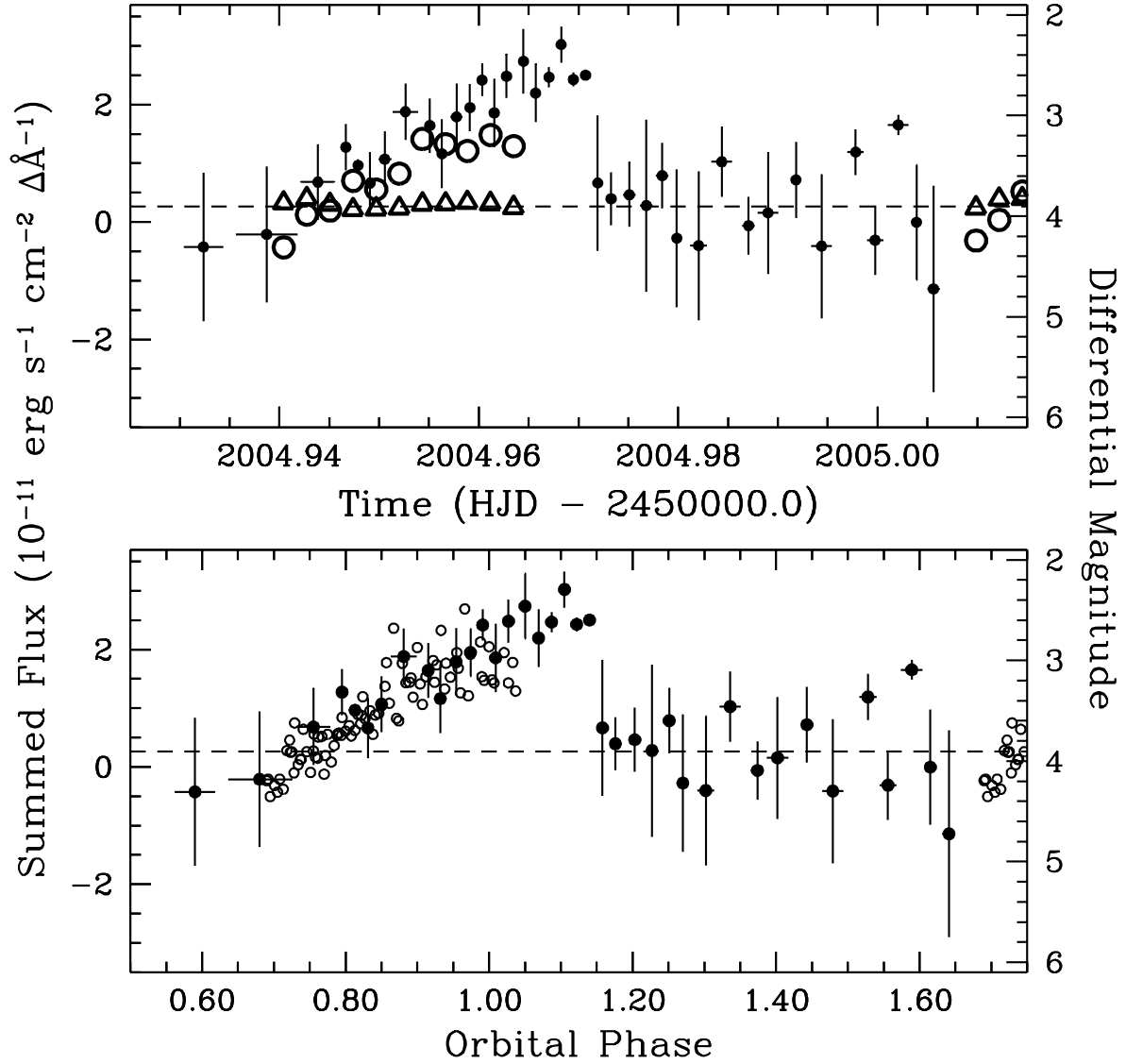


Fig. 3.— Optical and FUV light curves of VV Pup. The optical data are presented as in Figure 2. In the top panel, the FUV continuum (large unfilled circles) and emission (large unfilled triangles) flux data are overplotted for the *FUSE* visits that exactly overlap the time range of the optical observations. In the bottom panel, the FUV continuum flux data (small unfilled circles), folded on the ephemeris of Walker (1965), are overplotted. The vertical axes on the left in both panels give the flux scale; the vertical axes on the right in both panels give the optical magnitude scale. The range of the flux axis has been chosen so that the phase-folded continuum flux points most closely overlap the optical data (assuming that the start of the continuum flux data corresponds to the “zero” level of the optical light curve).

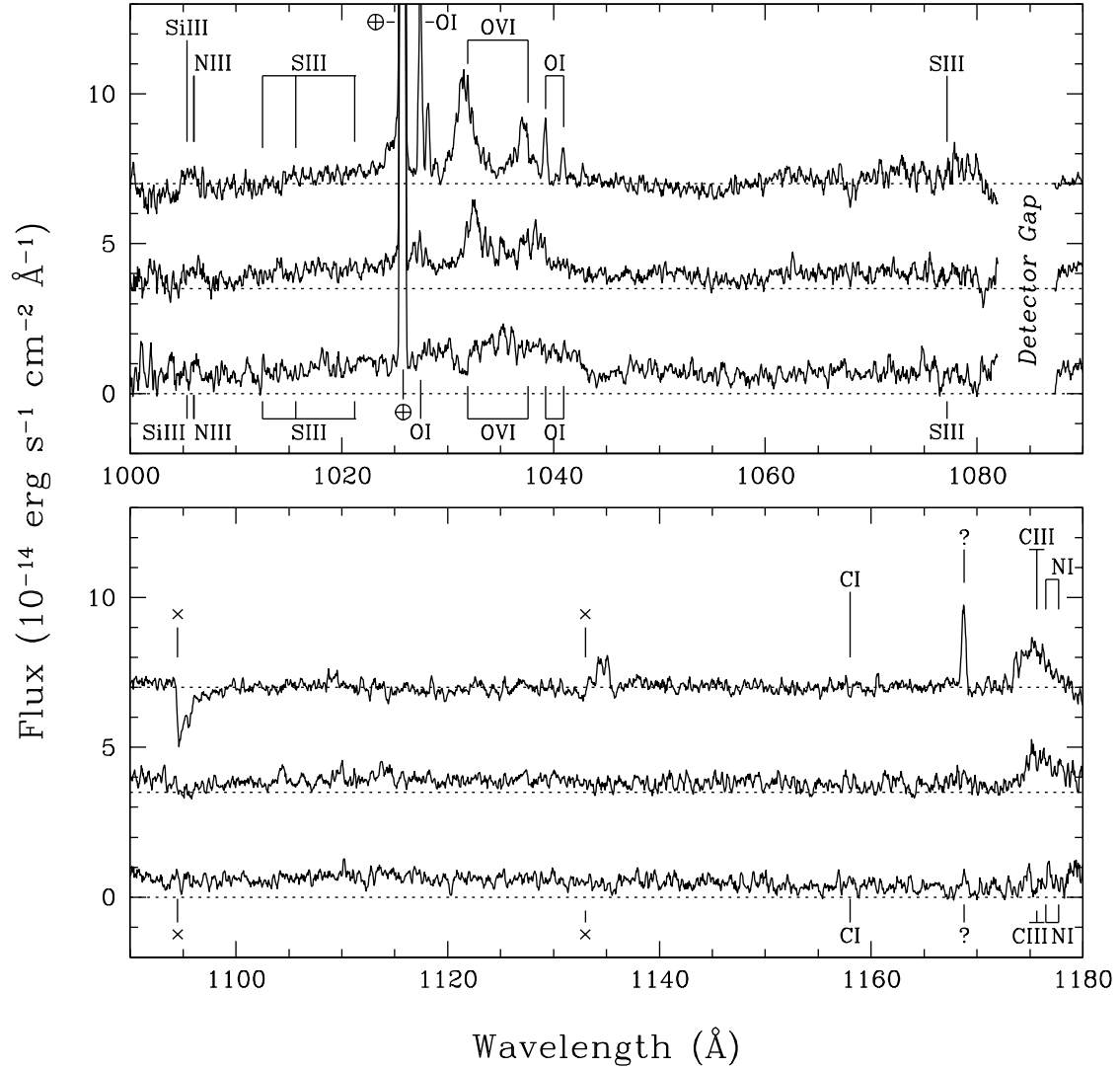


Fig. 4.— Time-resolved FUV spectra of VV Pup. The top panel shows the wavelength range 1000–1090 Å, the bottom panel shows 1090–1180 Å. The spectra were rebinned to a uniform dispersion of  $0.05 \text{ \AA pixel}^{-1}$  during processing, and have been boxcar smoothed by 5 pixels in this figure. The three spectra correspond to phase ranges of  $\Delta\phi_1 = 0.67\text{--}0.79$  (upper spectrum in each panel),  $\Delta\phi_2 = 0.80\text{--}0.89$  (middle), and  $\Delta\phi_3 = 0.90\text{--}0.06$  (bottom). The bottom spectrum in each panel shows the true flux level, while the other spectra have been successively offset by  $+2.5 \times 10^{-14} \text{ erg s}^{-1} \text{ cm}^{-2} \text{ \AA}^{-1}$  (the dotted lines show the true zero level for each spectrum). A number of line transitions have been identified and marked with vertical bars; multiplet transitions of the same ion are joined by a horizontal bar. The features marked “ $\times$ ” may be artifacts, since they are located near the ends of detector segments. The feature at 1168 Å marked “?” possibly corresponds to He I  $\lambda 584$  in second order (Feldman et al. 2001).

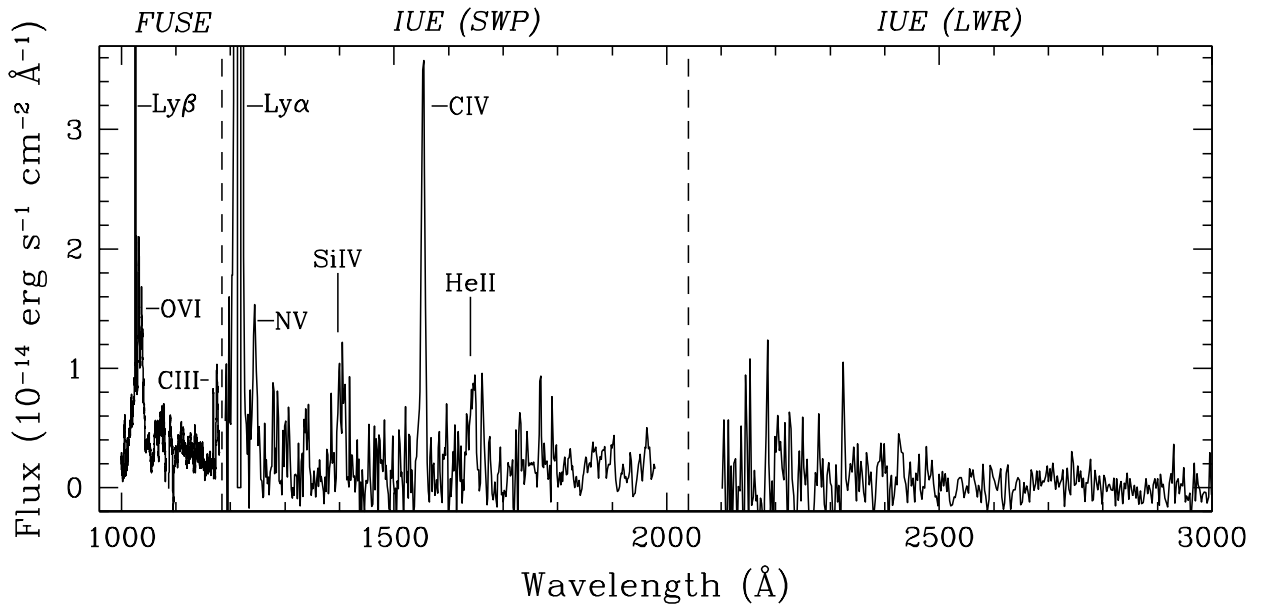


Fig. 5.— Combined *FUSE* and *IUE* spectra of VV Pup. The *IUE* spectra are SWP07868 (14,400 s obtained on 1980 February 04) and LWR07309 (7200 s obtained on 1980 March 26). Vertical dashed lines mark the boundaries between the *FUSE*, *IUE* SWP, and *IUE* LWR wavelength regions. Several spectral features are indicated.

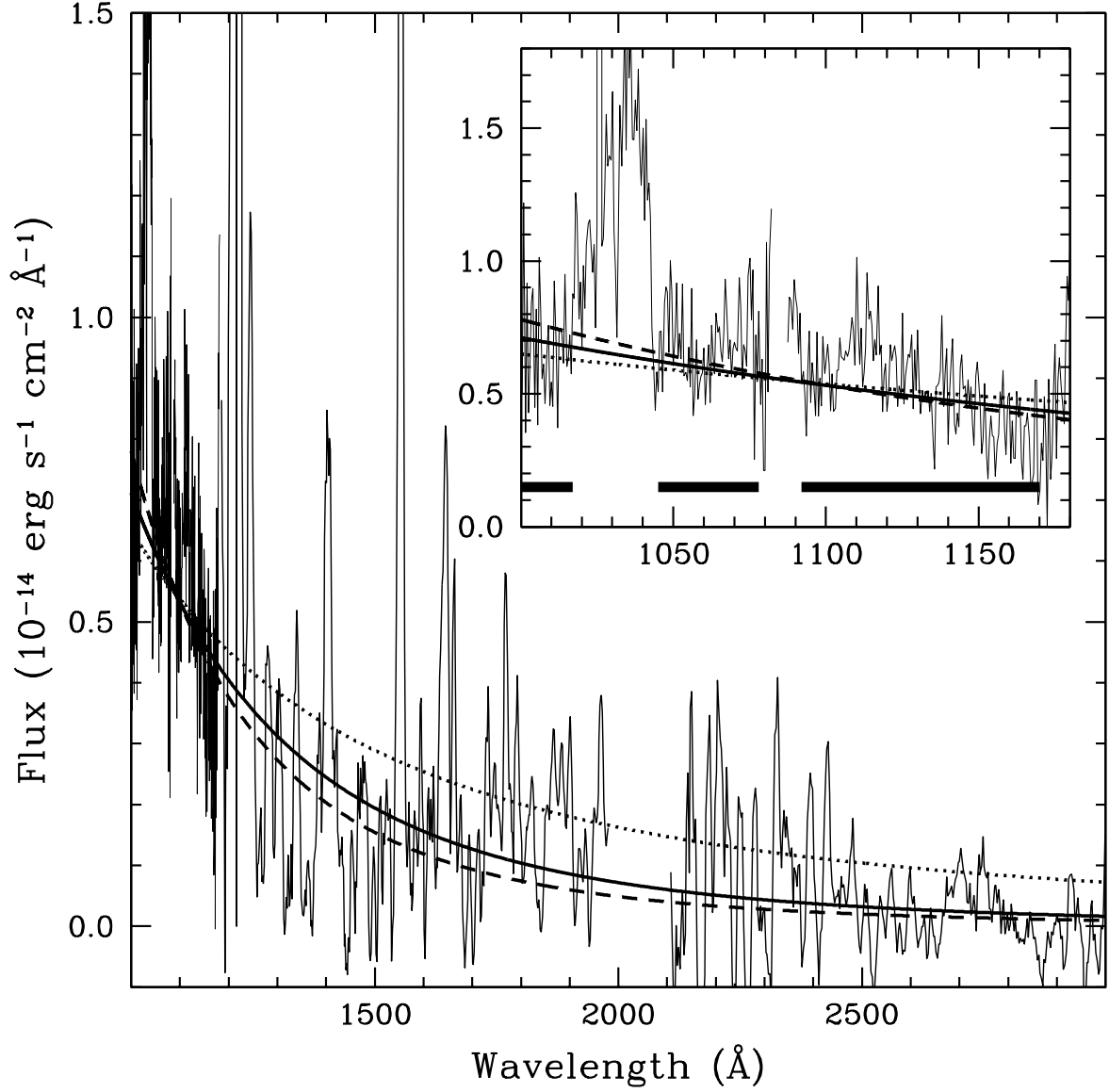


Fig. 6.— Main panel shows the  $\Delta\phi_3 = 0.90 - 0.06$  spectrum from Figure 4 (rebinned to a dispersion of  $0.5 \text{ \AA pix}^{-1}$ ) and the *IUE* spectra of VV Pup from Figure 5 (faint solid line) with three representative models: a power law of the form  $F_\lambda \propto \lambda^\alpha$  where  $\alpha = -2$  (dotted line) or  $-4$  (dashed line), and a blackbody function with  $T_{\text{bb}} = 90,000 \text{ K}$  (dark solid line). The inset panel shows a close-up of only the *FUSE* spectrum with the same three models. The horizontal bars show the wavelength ranges used for determining the scaling factors that best fit each model to the *FUSE* data (i.e., the *IUE* data were *not* used to normalize the models). Bright airglow lines (and the C IV  $\lambda 1550$  emission line) are truncated in both plots. The *IUE* spectra have been boxcar-smoothed by 5 pixels.